


Relativistic head-on collisions of $U(1)$ gauged Q -ballsMichael P. Kinach^{✉*} and Matthew W. Choptuik^{✉†}*Department of Physics and Astronomy, University of British Columbia,
6224 Agricultural Road, Vancouver, British Columbia V6T 1Z1, Canada* (Received 9 April 2024; accepted 4 June 2024; published 9 July 2024)

We investigate the collision dynamics of $U(1)$ gauged Q -balls by performing high-resolution numerical simulations in axisymmetry. Focusing on the case of relativistic head-on collisions, we consider the effects of the initial velocity, relative phase, relative charge, and electromagnetic coupling strength on the outcome of the collision. We find that the collision dynamics can depend strongly on these parameters; most notably, electromagnetic effects can significantly alter the outcome of the collision when the gauge coupling is large. When the gauge coupling is small, we find that the dynamics generally resemble those of ordinary (nongauged) Q -balls.

DOI: [10.1103/PhysRevD.110.015012](https://doi.org/10.1103/PhysRevD.110.015012)**I. INTRODUCTION**

The study of nonlinear wave equations has a long and rich history in modern physics. One of the most remarkable insights to emerge from this tradition has been the discovery of *solitons*: localized solutions to the field equations that can propagate without dispersing. In many respects, solitons behave like a rudimentary model of a particle which can be constructed from smooth classical fields. They can generally be classified as either topological or nontopological depending on whether the underlying model has a nontrivial topology. Examples of topological solitons include the kink/antikink solutions of quantum field theory, skyrmions and vortices in condensed matter physics, and cosmological domain walls [1,2]. In contrast, nontopological solitons can arise due a balancing between the effects of nonlinearity and dispersion and are often characterized by the existence of a conserved Noether charge [2]. The prototypical examples of nontopological solitons are Q -balls which arise in complex scalar field theories admitting a $U(1)$ symmetry.

The study of Q -balls began in earnest with the work of Coleman [3] who described them as localized solutions of a complex scalar field theory with a nonlinear attractive potential and a global $U(1)$ symmetry. This work has since been extended to show that Q -ball solutions can arise in a variety of physically motivated models (see [4] for a

review). In the context of cosmology and particle physics, Q -balls may be relevant for various early Universe scenarios such as baryogenesis and the dark matter problem [5–8]. They may also arise in the context of nonlinear optics [9] and condensed matter systems [10,11]. Mathematically, Q -balls are characterized by the presence of a conserved Noether charge Q which is associated with the $U(1)$ symmetry of the theory. The global $U(1)$ symmetry can also be made into a local $U(1)$ symmetry via the introduction of a $U(1)$ gauge field; the resulting solutions are called *gauged Q -balls* and represent a coupling of the system to electromagnetism [12].

While the basic properties of Q -balls are well known, it remains a challenging problem to model their full time-dependent dynamical behavior. This is due mainly to the nonlinear structure of the underlying equations which typically requires a numerical treatment. Early work on this topic revealed that Q -ball dynamics can be remarkably complex, particularly when considering interactions and relativistic collisions of Q -balls. Perhaps the most comprehensive studies of this type were performed by Axenides *et al.* in two spatial dimensions [13] and Battye and Sutcliffe in three spatial dimensions [14]. There it was shown that Q -balls can interact elastically or inelastically depending on the collision parameters. They may also transfer charge, annihilate, or form oscillatory charge-swapping structures [15–17] under the right conditions. Additional studies have also considered different scalar field models, higher collision velocities, or greater numerical resolutions [18–22]. A general conclusion to be drawn from these studies is that Q -ball behavior can be quite complex and unexpected.

In the present paper, we continue this exploration of Q -ball dynamics by considering relativistic head-on collisions of $U(1)$ gauged Q -balls in axisymmetry. Intuitively, one might expect that the addition of the $U(1)$ gauge field may lead to

*Contact author: mikin@physics.ubc.ca†Contact author: choptuik@physics.ubc.ca

Published by the American Physical Society under the terms of the Creative Commons Attribution 4.0 International license. Further distribution of this work must maintain attribution to the author(s) and the published article's title, journal citation, and DOI. Funded by SCOAP³.

novel dynamical behavior due to the interaction of electromagnetic charges and currents. However, this possibility has remained largely unexplored in the literature. Our aim is to shed light on this topic by performing fully nonlinear numerical evolutions of the field equations in axisymmetry. We explore the effects of various collision parameters such as the initial velocity, relative phase, relative charge, and electromagnetic coupling strength in order to gain insight on the general phenomenology of gauged Q -ball collisions.

In a previous paper [23], we numerically investigated the dynamical behavior of $U(1)$ gauged Q -balls when subject to axisymmetric perturbations. There it was found that stable gauged Q -ball configurations can exist in both logarithmic and polynomial models. Using these solutions as a starting point, we construct binary gauged Q -ball initial data consisting of two stable solutions which are boosted toward each other at relativistic velocities. We then evolve the system according to the equations of motion and observe the subsequent dynamics.

When the gauge coupling is small, our results parallel those found for ordinary (nongauged) Q -ball collisions. Specifically, we find that the collision dynamics can be divided into three regimes—which we will call the *elastic*, *fragmentation*, and *merger* regimes—depending on the incident velocity of the colliding Q -balls. In the elastic regime (corresponding to high velocities), the collisions are primarily elastic with the Q -balls passing through each other virtually unscathed and forming a destructive interference pattern at the moment of impact. In the merger and fragmentation regimes (corresponding to low and intermediate velocities, respectively), the collisions are primarily inelastic with several possible outcomes. At the lowest velocities, the Q -balls can merge into a single Q -ball of a larger size, while at intermediate velocities they tend to fragment into many pieces. We also investigate collisions of oppositely charged and phase-shifted Q -balls, finding evidence for annihilation and charge transfer, respectively.

When the gauge coupling is large, we find that electromagnetic effects can significantly alter the outcome of the collision. For gauged Q -balls with charge of equal sign, we find that the Coulomb repulsion tends to decelerate the Q -balls prior to the moment of impact. At low incident velocities, this can prevent the interaction of the Q -ball fields entirely; at higher velocities, it simply reduces the effective collision velocity. We also find that collisions at large gauge coupling are rarely an elastic process. Unlike the free-passage behavior observed for small gauge coupling, the collision of gauged Q -balls at high-velocities tends to result in the formation of ringlike objects (which we have previously called “gauged Q -rings” [23]) or elongated structures even for collision velocities very close to the speed of light. For collisions involving Q -balls of unequal phase, we again observe charge transfer similar to the case of small gauge coupling. However, we find that the gauged Q -balls created in this process often break apart,

presumably due to the reduced range of stable solutions which exist at large gauge coupling. For collisions of oppositely charged Q -balls, the Coulomb force accelerates the Q -balls prior to the moment of impact. These collisions can result in the annihilation of significant charge and the production of an electromagnetic radiation pulse. In sum, we find that the collision of gauged Q -balls can be a violent process with some striking differences when compared to the nongauged case.

The outline of this paper is as follows: in Sec. II, we briefly review the theory of $U(1)$ gauged Q -balls. In Sec. III, we summarize our numerical approach to the head-on collision problem. In Sec. IV, we present our main results and summarize the general dynamics observed for $U(1)$ gauged Q -ball collisions. In Sec. V, we provide some concluding remarks.

In this work, we use units where $c = \hbar = 1$ and employ the metric signature $(-, +, +, +)$. For brevity, we will interchangeably use the terms “ Q -ball” and “gauged Q -ball” when referring to Q -balls coupled to the electromagnetic field. When referring to Q -balls which do not admit any such coupling, we will explicitly use the term “nongauged Q -ball.”

II. REVIEW OF $U(1)$ GAUGED Q -BALLS

For a system composed of a complex scalar field ϕ coupled to a $U(1)$ gauge field, A_μ , the Lagrangian density takes the form

$$\mathcal{L} = -(D_\mu \phi)^* D^\mu \phi - V(|\phi|) - \frac{1}{4} F_{\mu\nu} F^{\mu\nu}. \quad (1)$$

Here, $F_{\mu\nu} = \partial_\mu A_\nu - \partial_\nu A_\mu$ is the electromagnetic field tensor, $D_\mu = \nabla_\mu - ieA_\mu$ describes the gauge covariant derivative with coupling constant e , and $V(|\phi|)$ represents a $U(1)$ -invariant scalar field potential. The equations of motion for the theory (1) take the form

$$D_\mu D^\mu \phi - \frac{\partial}{\partial \phi^*} V(|\phi|) = 0, \quad (2)$$

$$\nabla_\mu F^{\mu\nu} + e j^\nu = 0, \quad (3)$$

where j^ν is the Noether current density,

$$j^\nu = -i(\phi^* D^\nu \phi - \phi (D^\nu \phi)^*). \quad (4)$$

This quantity can be integrated to obtain the conserved Noether charge $Q = \int j^0 d^3x$ associated with the $U(1)$ symmetry of the theory. Likewise, there exists a conserved energy $E = \int T_{00} d^3x$ which can be computed from the energy-momentum tensor of the theory,

$$T_{\mu\nu} = F_{\mu\alpha} F_{\nu\beta} g^{\beta\alpha} - \frac{1}{4} g_{\mu\nu} F_{\alpha\beta} F^{\alpha\beta} + D_\mu \phi (D_\nu \phi)^* + D_\nu \phi (D_\mu \phi)^* - g_{\mu\nu} (D_\alpha \phi (D^\alpha \phi)^* + V(|\phi|)). \quad (5)$$

Solutions to the equations of motion (2)–(3) which represent gauged Q -balls can be found by making a spherically symmetric ansatz for the fields,

$$\phi(t, \vec{x}) = f(r)e^{i\omega t}, \quad (6)$$

$$A_0(t, \vec{x}) = A_0(r), \quad (7)$$

$$A_i(t, \vec{x}) = 0, \quad (8)$$

and imposing the boundary conditions

$$\lim_{r \rightarrow \infty} f(r) = 0, \quad \frac{df}{dr}(0) = 0, \quad (9)$$

$$\lim_{r \rightarrow \infty} A_0(r) = 0, \quad \frac{dA_0}{dr}(0) = 0. \quad (10)$$

This ansatz yields the reduced equations of motion

$$f''(r) + \frac{2}{r}f'(r) + f(r)g(r)^2 - \frac{1}{2} \frac{d}{df} V(f) = 0, \quad (11)$$

$$A_0''(r) + \frac{2}{r}A_0'(r) + 2ef(r)^2g(r) = 0, \quad (12)$$

where we have defined $g(r) = \omega - eA_0(r)$. There are several approaches to finding solutions which satisfy the coupled equations (11)–(12) such as shooting [12], relaxation [24], or via mapping from the profiles of nongauged Q -balls [25]. Here we utilize an iterative shooting procedure to numerically determine $f(r)$ and $A_0(r)$ which satisfy (11)–(12) to a good approximation. Further details about this technique are provided in [23].

III. NUMERICAL APPROACH

As a starting point for our evolution, we consider the line element

$$ds^2 = -dt^2 + d\rho^2 + \rho^2 d\varphi^2 + dz^2, \quad (13)$$

where (t, ρ, φ, z) are the standard cylindrical coordinates. Further, we impose axisymmetry on the system by requiring all dynamical variables to be φ -independent. This is done purely to reduce the computational cost of modeling the system in fully three spatial dimensions. With this choice, the equations of motion (2)–(3) can be expressed as a set of six coupled nonlinear partial differential equations; these equations are identical to those listed in the appendix of our previous paper [23]. Working in the Lorenz gauge, the equations of motion are supplemented with the gauge condition

$$\nabla_\mu A^\mu = 0, \quad (14)$$

and the equations

$$\nabla_i E^i = ej^0, \quad (15)$$

$$\nabla_i B^i = 0, \quad (16)$$

where E^i and B^i are the (three-dimensional) electric and magnetic field vectors, respectively, whose components are determined via the electromagnetic field tensor, $F_{\mu\nu}$. Together, the Eqs. (14)–(16) act as additional constraints on the evolution: it is expected that a numerical solution to the equations of motion will approximately satisfy these constraint equations at any given time.

In order to construct initial data which is suitable for studying head-on collisions, we interpolate a pair of spherically symmetric gauged Q -ball solutions in the $\rho - z$ plane using Neville's algorithm to fourth-order in the mesh spacing [26]. The center of each Q -ball is chosen to coincide with the line $\rho = 0$ in order to preserve the spherical symmetry of each Q -ball in the binary. Each Q -ball is also given an initial displacement along the z -axis so that the binary is well-separated at the initial time. Finally, we apply a Lorentz boost to each Q -ball along the z -direction at a relativistic speed v (where $v = 1$ corresponds to the speed of light in our units) so that they travel toward each other. After these operations, the field variables $f \in \{\phi, \partial_t \phi, A_\mu, \partial_t A_\mu\}$ are initialized according to the linear superposition

$$f(\rho, z) = f_A(\rho, z) + f_B(\rho, z), \quad (17)$$

subject to the condition

$$f_A(\rho, z) \cdot f_B(\rho, z) \approx 0, \quad (18)$$

where the subscripts $\{A, B\}$ identify each individual Q -ball in the binary.

Practically speaking, the condition (18) is not trivial to satisfy in general. While the scalar field falls off exponentially away from the Q -ball center (thereby satisfying the condition even at modest separation distances), the same cannot be said for the gauge field, which falls off like $1/r$. This long-range behavior inherently introduces violations of the constraint equations (14)–(16) when the gauge fields of each Q -ball significantly overlap. The magnitude of this violation depends on several factors such as the initial separation distance, the boost velocity, and the total charge of the constituent Q -balls. To deal with this problem, we implement an FAS multigrid algorithm [26] to re-solve the equations (15)–(16) at the initial time and minimize the constraint violation for arbitrary superpositions of the form (17). We also monitor the residuals of the constraint equations (14)–(16) during the evolution to ensure that they do not grow significantly over the timescales under consideration.

For the purposes of this work, we choose several representative examples of gauged Q -ball solutions to

TABLE I. Table of several gauged Q -ball solutions used in our collision simulations. The solutions LogA, LogB and LogC correspond to the logarithmic potential (19) while PolyA and PolyB correspond to the polynomial potential (20). From left to right, the remaining columns indicate the value of the electromagnetic coupling constant e , the initial central value of the scalar field $|\phi(0,0)|$, the initial central value of the gauge field $A_0(0,0)$, the Q -ball oscillation frequency ω , the total energy E of the solution (when stationary), and the total Noether charge $|Q|$ of the solution.

Solution	e	$ \phi(0,0) $	$A_0(0,0)$	ω	E	$ Q $
LogA	0.1	0.3669	2.697×10^{-2}	2.003	6.769	3.006
LogB	0.1	1.627	0.2682	1.027	45.45	30.03
LogC	1.1	0.6461	1.383	2.522	52.08	22.37
PolyA	0.02	2.062	0.4353	0.6587	476.4	582.9
PolyB	0.17	1.973	2.515	0.9976	405.1	387.5

act as initial data for the colliding binaries. The properties of these solutions are listed in Table I. In our simulations, we consider two different possibilities for the scalar field potential $V(|\phi|)$ in the model (1). These are

$$V_{\log}(|\phi|) = -\mu^2 |\phi|^2 \ln(\beta^2 |\phi|^2), \quad (19)$$

$$V_6(|\phi|) = m^2 |\phi|^2 - \frac{k}{2} |\phi|^4 + \frac{h}{3} |\phi|^6, \quad (20)$$

where μ , β , m , k , and h are real, positive parameters. In Table I, the solutions pertaining to the logarithmic potential (19) are named LogA, LogB, and LogC while the solutions due to the polynomial potential (20) are named PolyA and PolyB. These solutions, which are known to be stable against axisymmetric perturbations [23], are specifically chosen to illustrate the range of dynamical features associated with head-on collisions of gauged Q -balls. We emphasize that aside from the examples listed in Table I, we have also studied collisions involving several other configurations and find the dynamics to be consistent with the results reported below.

In addition to varying the scalar potential, we also adjust the values of the electromagnetic coupling constant e , the initial velocity v , the relative phase difference α , and the relative sign of the Noether charge Q for the colliding Q -balls. The value of α is set through a simple modification of the spherical Q -ball ansatz (6):

$$\phi(t, \vec{x}) = f(r) e^{(i\omega t) + i\alpha}, \quad (21)$$

where $\alpha \in [0, \pi]$ and $\epsilon = \pm 1$. Since we only consider collisions between Q -balls with identical ω , the value of α determines the relative difference in phase between the colliding Q -balls prior to the moment of impact. The sign of ϵ , meanwhile, provides a mechanism through which we can study both Q -ball/ Q -ball and Q -ball/anti- Q -ball

collisions. This can be understood from the fact that the sign of the Noether charge Q (and the sign of the electric charge $Q_e = eQ$) of a gauged Q -ball is connected to the sign of the oscillation frequency ω [24]. Therefore, adjusting the sign of ϵ for one Q -ball in the binary [as well as taking $A_0(r) \rightarrow -A_0(r)$ in (7)] effectively flips the sign of its charge, allowing us to superpose initial data of equal or opposite charge as desired.

After specifying the initial data at $t = 0$, we proceed by evolving the system forward in time. To facilitate this, we invoke a coordinate transformation $x^\mu = (t, \rho, z) \rightarrow x^{\mu'} = (t, P, Z)$ according to

$$\rho = d \exp(cP) - d \exp(-cP), \quad (22)$$

$$z = d \exp(cZ) - d \exp(-cZ), \quad (23)$$

where c and d are positive, real parameters. With appropriate choice of c and d , the transformation (22)–(23) remains approximately linear near the origin while becoming increasingly compactified at large coordinate values. This is an attractive feature for our numerical domain because it allows us to resolve the dynamics at large length scales without incurring an excessive computational cost. To perform the evolution in this coordinate system, we use a second-order Crank-Nicolson finite-difference scheme implemented with fourth-order Kreiss-Oliger dissipation as a smoothing operator. A modified Berger-Oliger adaptive mesh refinement (AMR) algorithm [27] is used to dynamically increase the numerical resolution of our simulations in the regions of greatest interest. For all results presented below, the base grid is taken to be 129 by 257 grid points in $\{P, Z\}$ with up to 8 levels of additional mesh refinement at a refinement ratio of 2:1. We choose a Courant factor of $\lambda = dt / \min\{dP, dZ\} = 0.25$. At the outer boundaries, we impose outgoing (Sommerfeld) boundary conditions in order to accommodate the long-range behavior of the electromagnetic field and reduce the effects of spurious boundary noise. In addition, we apply reflective or antireflective boundary conditions as necessary along the axis of symmetry in order to enforce regularity.

For numerical convenience, we choose $\mu = \beta = m = k = 1$ and $h = 0.2$ in (19)–(20) following our previous work [23]. We select $c = 0.05$, $d = 10$ in (22)–(23) and set the domain boundaries to span at least $\{P: 0 \leq P \leq 50\}$ and $\{Z: -50 \leq Z \leq 50\}$ which corresponds to $\{\rho: 0 \leq \rho \lesssim 121\}$ and $\{z: -121 \lesssim z \lesssim 121\}$ in the original coordinate system. With this choice, we find the numerical domain to be large enough to capture the relevant post-collision dynamics of the Q -balls. We emphasize that while all evolutions have been performed using the compactified coordinates P and Z , we will hereafter present all results using the linear coordinates ρ and z . This is done primarily to facilitate the interpretation of the results. Finally, since the numerical code is identical to the one used in [23]

TABLE II. Summary of the main dynamical results from our collision simulations. Shown are the observed collision outcomes (classified by either “small” or “large” values of the gauge coupling constant e) as a function of various collision parameters: the relative Noether charge Q of the colliding binary (either equal or opposite), the relative phase difference α , and the collision velocity v (heuristically divided into “low-velocity”, “intermediate-velocity”, and “high-velocity” regimes). We comment that the results listed in this table together capture the dynamics in both the logarithmic (19) and polynomial (20) scalar field models. These results are explained in further detail throughout Sec. IV.

Collision parameters			Result	
Relative charge Q	Phase difference α	Collision velocity v	Small e	Large e
Equal Q	$\alpha = 0$	Low v	Merger	Coulomb repulsion (no collision)
		Intermediate v	Merger, fragmentation	Merger, fragmentation
		High v	Free-passage	Fragmentation
	$\alpha \in (0, \pi)$	Low v	Charge transfer	Coulomb repulsion (no collision)
		Intermediate & High v		Charge transfer, fragmentation
	$\alpha = \pi$	Low v	Phase repulsion	Coulomb repulsion (no collision)
	Intermediate & High v		Phase repulsion	
Opposite Q	All α	All v	Partial annihilation	Partial annihilation, radiation emission

(aside from applying the coordinate transformation (22)–(23) and the generation of binary initial data), we refer the reader to [23] for issues of code validation such as convergence and independent residual tests.

IV. NUMERICAL RESULTS

We now describe the results of our numerical experiments. In our collision simulations, we consider the effects of the following parameters on the resulting dynamics: gauge coupling strength e , collision velocity v , relative phase difference α , and relative sign of the Noether charge Q . In most cases, we restrict the collision velocity to the range $0.1 \leq v \leq 0.9$ and the phase difference to $\alpha \in \{0, \pi/4, \pi/2, 3\pi/4, \pi\}$, though in some cases we explore beyond these values to get a complete picture of the dynamics. Further, we test the effects of the choice of scalar potential [logarithmic (19) versus polynomial (20)] as well as the difference between colliding Q -balls of equal charge and opposite charge. We note that for all simulations presented below, the constituent Q -balls are always composed of identical charge magnitudes (i.e., we do not present any results for collisions between Q -balls of differing $|Q|$). For comparison purposes, we first explore the results at small gauge coupling. We then move on to the case where the gauge field is strongly coupled to highlight the salient dynamics. For presentation purposes, we have relegated some plots of the dynamics in this section to the Appendix.

We provide in Table II a broad, high-level overview of the main results of our numerical experiments. We will devote the remainder of this work to discussing the various phenomena which are reflected in the table.

A. Small gauge coupling

Here we consider collisions involving solutions LogA, LogB, and PolyA from Table I. Since the strength of the

gauge coupling is small in these cases (see [28] where this notion is made precise), it is expected that the dynamics of gauged Q -balls in this regime will be similar to the dynamics of ordinary (nongauged) Q -balls.

Let us begin by discussing the effect of Q -ball velocity on the outcome of the collision. In previous studies [13,14,21] it has been shown that the dynamics of equal-charge, nongauged Q -ball collisions can generally be divided into three regimes: (i) at low velocities, a “merger” regime wherein the Q -balls tend to coalesce, (ii) at intermediate velocities, a “fragmentation” regime wherein the Q -balls tend to break up into smaller components, and (iii) at high velocities, an “elastic” regime wherein the Q -balls tend to pass through each other virtually unscathed. We find that gauged Q -ball collisions with small gauge coupling are generally consistent with these previous findings.

First, consider the low-velocity regime. In Fig. 1, we plot the collision of two Q -balls of type LogA (see Table I) with equal charge, velocity $v = 0.1$, and phase difference $\alpha = 0$. As the Q -balls collide, they merge temporarily before separating again and propagating a short distance along the axis of symmetry. However, they have insufficient kinetic energy to completely escape their mutual influence and instead repeatedly merge and partially separate. Small amounts of scalar matter are also released during this process. As the evolution proceeds, the field configuration settles down into a single coherent merged state. The final Q -ball is of a larger total size than LogA and remains at the origin lightly perturbed.

When boosted to velocities above a certain threshold, the colliding Q -balls have sufficient kinetic energy to avoid a merged final state (for LogA, the velocity threshold is $v \gtrsim 0.125$). At these “intermediate” velocities, a significant quantity of the initial charge of each Q -ball continues propagating along the axis of symmetry after the collision.

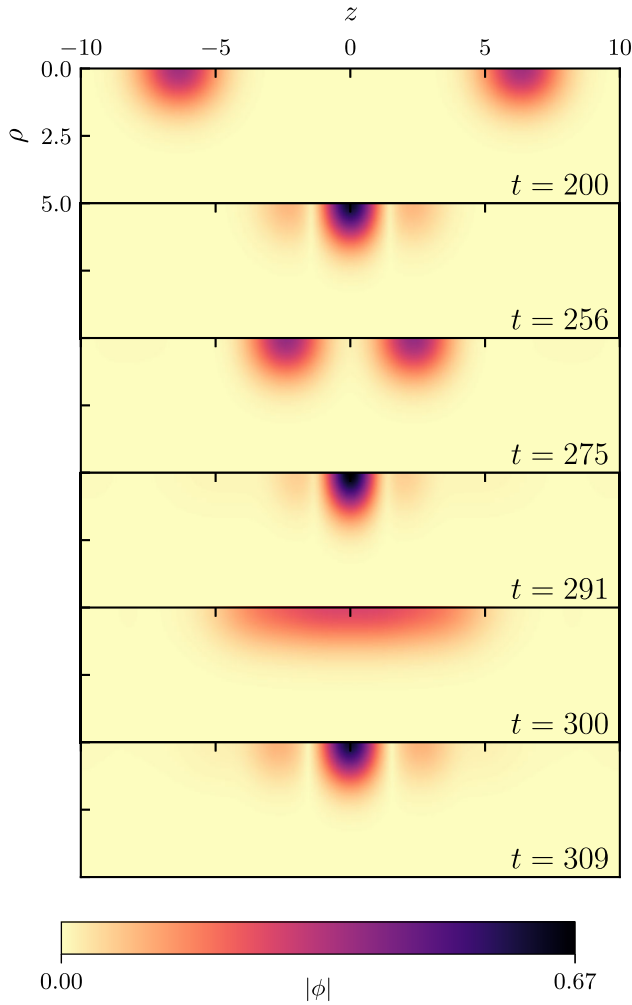


FIG. 1. Evolution of the scalar field modulus $|\phi|$ for a collision of solutions of type LogA with equal charge, velocity $v = 0.1$, and phase difference $\alpha = 0$. The Q -balls collide at $t \approx 250$ and repeatedly merge and separate. By $t \approx 600$ (beyond what is shown here), the field configuration settles down into a single larger Q -ball which remains perturbed at the origin.

These resulting Q -balls are highly perturbed and oscillatory. In most cases, this process also results in some relic amount of charge left behind: the Q -balls have partially fragmented into smaller structures. These smaller Q -balls may either remain stationary at the origin or continue to propagate along the axis of symmetry, lagging the main Q -balls at a lower velocity. An example of such a collision for solution LogA at velocity $v = 0.5$ is given in the Appendix (Fig. 12).

At the highest velocities, collisions between the Q -balls are primarily elastic and they emerge from the collision relatively unscathed. An illustration of this phenomenon is given in the Appendix (Fig. 13) for solution LogA at velocity $v = 0.9$. It is also in this regime that the wavelike nature of Q -balls becomes readily apparent through the appearance of interference fringes at the moment of impact.

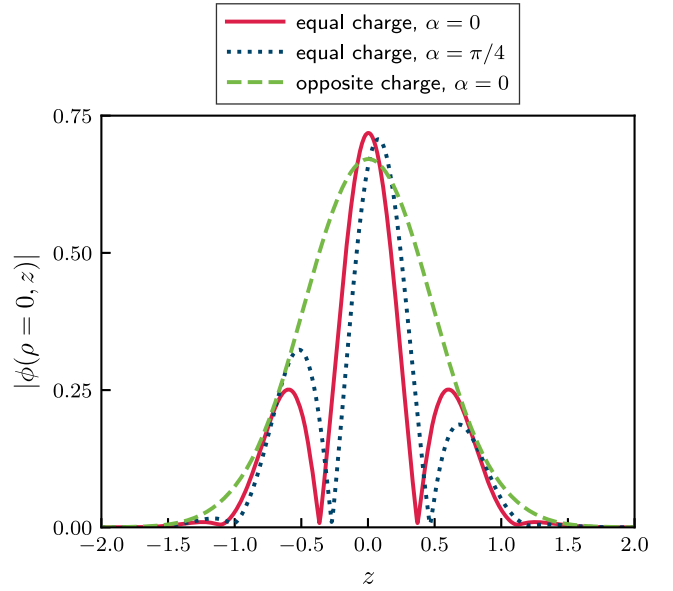


FIG. 2. Profiles of the scalar field modulus $|\phi|$ evaluated along the axis of symmetry during collisions involving solution LogA with $v = 0.9$. Three cases are shown: an equal-charge collision with no phase difference ($\alpha = 0$), an equal-charge collision with phase difference $\alpha = \pi/4$, and an opposite-charge collision with no phase difference ($\alpha = 0$). In each case, the profile is shown at the moment $|\phi|$ reaches its maximal value. For collisions with equal charge, a destructive interference pattern forms at the moment of impact. For collisions with opposite charge, the interference pattern is purely constructive.

Plotted in Fig. 2 are the interference fringes observed for collisions of solution LogA at $v = 0.9$. For equal-charge collisions, a clear fringe pattern emerges with fringe spacing inversely proportional to the collision velocity. Also shown are the effects of opposite-charge and phase-difference collisions on the fringe pattern (to be discussed below).

We now comment on the effects of phase difference on the collision dynamics. Recall that a phase difference is introduced into the system by choosing $\alpha \neq 0$ in (21). Since the colliding Q -balls in our study always have identical values of ω , this phase difference is preserved until the moment of impact regardless of the initial separation distance or initial velocity. As reported previously [14], the main effect of this phase difference is to induce charge transfer between the colliding Q -balls. This behavior can be understood in terms of relative phase accelerations [14] or the induced rate of change of momentum for the colliding Q -balls [29]. Testing the effects of phase difference at $\alpha \in \{0, \pi/4, \pi/2, 3\pi/4, \pi\}$, we find that charge transfer is generally maximized at the lowest collision velocities and for small phase differences, in agreement with previous studies.

Plotted in Fig. 3 is the collision of solution LogA at a velocity of $v = 0.1$ and a phase difference $\alpha = \pi/4$. Initially, the Q -balls are of equal charge. At the moment

of impact, the Q -ball with lagging phase (rightmost Q -ball in the figure) suddenly gains charge from the Q -ball with leading phase (leftmost Q -ball). Since Q -balls are extended structures, it can be difficult to precisely determine the total charge Q contained in the resulting objects. However, by integrating Q in the half-volumes $z > 0$ and $z < 0$ after the collision takes place, we can estimate by the deviation from symmetry that approximately 18% of the charge is transferred during this process. We note that the total charge Q over the simulation domain remains conserved to within 0.1% during the evolution. In addition to charge transfer, we observe that the velocities of the resultant Q -balls after the collision are no longer identical: the smaller Q -ball moves faster than the larger one. This can be understood as a straightforward consequence of linear momentum conservation.

At intermediate velocities, we observe the same qualitative behavior, though with the amount of charge transfer reduced (for instance, only $\sim 7\%$ is transferred at $v = 0.5$, $\alpha = \pi/4$ for solution LogA). In some cases, the charge transfer at these velocities is accompanied by the formation of one or more smaller Q -balls which remain along the axis of symmetry after the collision and lag the main Q -balls, being slightly perturbed. At the highest velocities, the charge transfer is minimal (for instance, $\sim 1\%$ or less of

the charge is transferred with $v \gtrsim 0.9$, $\alpha = \pi/4$ for solution LogA) and no significant smaller Q -balls are formed during the collision. However, the phase difference still manifests through a distortion of the interference fringes as illustrated in Fig. 2.

A notable exception to the charge transfer phenomenon occurs for completely out-of-phase collisions ($\alpha = \pi$). In this case, the Q -balls exhibit a purely repulsive interaction as they “bounce” off each other. At the moment of impact, the Q -balls are compressed in the boost direction and the value of $|\phi|$ temporarily grows by an amount which is proportional to the collision velocity. There is no charge transfer observed: the half-volumes $z > 0$ and $z < 0$ contain an identical amount of charge for all time. Note that this repulsive behavior for out-of-phase collisions has also been observed in other soliton models [30,31].

We now discuss collisions of oppositely charged Q -balls. These are the ones for which $\epsilon = -1$ in Eq. (21) for one of the Q -balls in the binary, resulting in a system composed of a gauged Q -ball and gauged anti- Q -ball. These collisions are predominantly characterized by the possibility of charge annihilation at the moment of impact, with the amount of annihilation depending on the collision velocity. For example, an opposite-charge collision corresponding to solution LogA at $v = 0.1$ results in $\sim 48\%$ of the charge annihilated. This situation is depicted in Fig. 4. The remaining charge emerges from the collision in the form of smaller Q -balls with a larger velocity. In addition, the relatively violent dynamics that occur during the annihilation leave them highly perturbed and oscillatory after the collision.

Charge annihilation during opposite-charge Q -ball collisions is also observed at larger velocities, though the amount of annihilation is reduced. For example, the amount of charge annihilated is $\sim 15\%$ at $v = 0.3$ and $\sim 7\%$ at $v = 0.5$ for solution LogA. In addition, the collision at these larger velocities is sometimes accompanied by the creation of smaller Q -balls remnants which remain along the axis of symmetry. At the highest velocities, the Q -ball/anti- Q -ball interaction results in very little annihilation (for example, only $\sim 1\%$ of charge is annihilated at $v = 0.9$). There are also fewer Q -ball remnants produced along the axis of symmetry and the fields interfere constructively at the moment of impact (see Fig. 2).

We have also tested the effects of phase difference on Q -ball/anti- Q -ball collisions, finding that it has a minimal influence on the dynamics. Charge transfer is not observed and the amount of annihilation is not significantly altered compared to the $\alpha = 0$ case.

Thus far, we have only discussed the dynamics associated with solution LogA. Now we turn to solution LogB in Table I. In this case, we find that a generic outcome of the collision is that the field values tend to grow without bound until the evolution becomes singular. This occurs even when the calculation is repeated using additional levels of

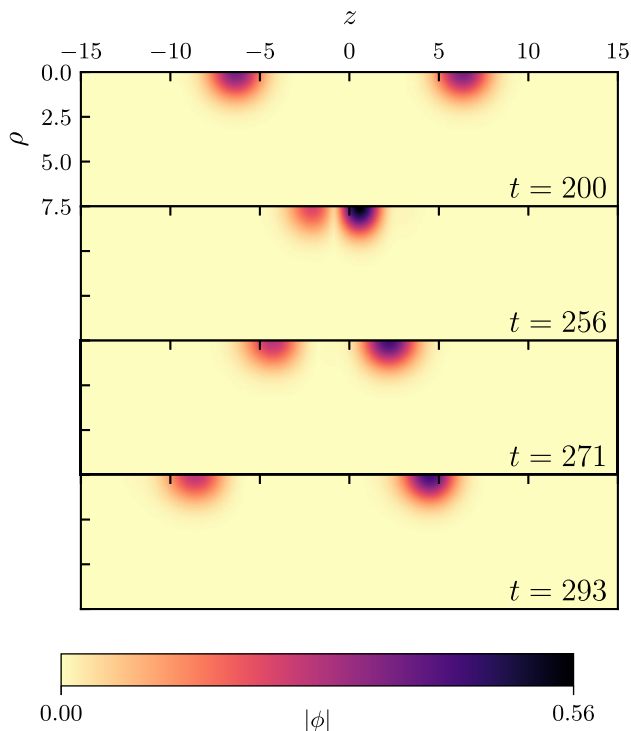


FIG. 3. Evolution of the scalar field modulus $|\phi|$ for a collision of solutions of type LogA with equal charge, velocity $v = 0.1$, and phase difference $\alpha = \pi/4$. After colliding at $t \approx 250$, the Q -ball with leading phase (left) transfers charge to the Q -ball with lagging phase (right). After the collision, the Q -balls have disparate velocities.

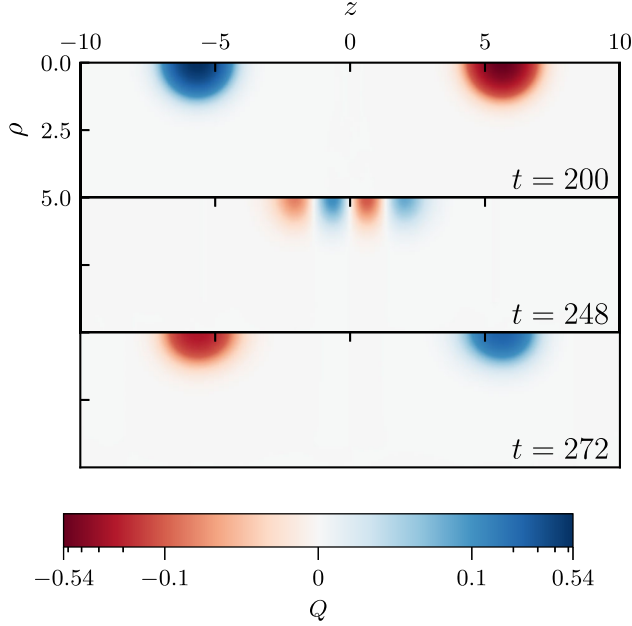


FIG. 4. Evolution of the Noether charge Q for a collision of solutions of type LogA with opposite charge, velocity $v = 0.1$, and phase difference $\alpha = 0$. The Q -balls collide at $t \approx 248$ and partially annihilate charge. After the collision, the resultant Q -balls pass through each other and continue propagating along the axis of symmetry with a larger velocity. Note that a hybrid color map is used: charge values below $|Q| = 0.1$ are mapped linearly to zero while values above this threshold are mapped logarithmically to the charge maximum.

mesh refinement. As discussed in [23], we can understand this behavior as a consequence of the logarithmic potential (19) being unbounded from below. In particular, for large scalar field values (such as those achieved at the moment of impact), the potential term $V(|\phi|)$ in (5) can become negative and may dominate over the other energies in the system. This can lead to the energy density becoming locally negative in the region of large $|\phi|$. At the same time, the energy density in other areas of the domain must grow so that the total integrated energy remains conserved to a positive quantity. This reciprocal process can result in runaway field growth which quickly causes the evolution to become singular. Due to such pathological effects, we do not consider collisions of Q -balls with sizes much larger than that of LogA for $e = 0.1$ in the logarithmic model.

To conclude this section, let us consider the collision dynamics under the polynomial potential (20). For this purpose, we will use solution PolyA in Table I as an illustrative example. Much like what is observed for solution LogA, we find that equal-charge collisions at low velocities are characterized by a merger regime. Notably, the range of velocities for which the Q -balls merge is quite large—in our experiments, merging occurs for $v \lesssim 0.7$. At higher collision velocities, the Q -balls have sufficient kinetic energy to escape the merged state and

continue propagating along the axis of symmetry after passing through each other. This is accompanied by a small portion of field content radiating away from the Q -balls after the moment of impact. We have also tested the effects of phase-difference and opposite-charge collisions involving solution PolyA, finding evidence for charge transfer and annihilation similar to what has been previously discussed.

B. Large gauge coupling

We now turn to collisions involving solutions LogC and PolyB from Table I. Unlike the collisions discussed in the previous section, these solutions involve a gauge coupling which is comparable in magnitude to the scalar potential parameters. We therefore expect that electromagnetic effects may have a nontrivial impact on the dynamics.

Once again, we begin by discussing the effect of the initial velocity on the outcome of the collision. Since the Q -balls can now carry a significant amount of electric charge, the long-range Coulomb force can influence the dynamics prior to the moment of impact. If the colliding Q -balls have equal charge, this results in deceleration and a corresponding decrease in their effective velocity before impact. If the colliding Q -balls have opposite charge, the result is acceleration which increases the effective velocity. In order to fully capture this behavior, it would be preferable to initialize the boosted Q -balls at $z = \pm\infty$ and let them travel toward each other. However, limitations in computational resources make it unfeasible to initialize the fields at arbitrarily large separation distances, so instead we initialize the Q -balls at $z = \pm 25$ for a given boost. As mentioned previously, we use a multigrid solver to remedy the unphysical constraint violations which may result from a simple superposition of the scalar and electromagnetic fields. In what follows, we will refer to the collision velocity as the velocity at which the Q -balls are initialized at $z = \pm 25$ rather than their effective velocity at the moment of impact.

To proceed with the analysis, we consider the solution LogC in Table I. Unlike what has been discussed in the case of LogA (corresponding to small gauge coupling), the dynamics of solution LogC during equal-charge collisions cannot be cleanly divided into a merger, fragmentation, and elastic regime. At low velocities, we find instead that the Coulomb repulsion is strong enough to completely prevent the scalar fields of each Q -ball from significantly interacting. This causes the Q -balls to decelerate as they approach each other, reach a turning point of vanishing velocity, and then accelerate away in the opposite direction. This behavior is found to occur for $0 < v \lesssim 0.3$. At velocities $v \gtrsim 0.3$, the Q -balls have sufficient kinetic energy to overcome the Coulomb repulsion and will eventually collide. In these situations, the general outcome is fragmentation of the gauged Q -ball into smaller components. Plotted in Fig. 5 is the collision of solution LogC at

$v = 0.55$. In contrast to the case of small gauge coupling (where no off-axis remnants were observed in the logarithmic model), here we see the formation of a distinct off-axis component which propagates outward before collapsing back onto the axis of symmetry at late times. As noted in [23], these off-axis components represent ring-like structures in three-dimensions which we call “gauged Q -rings”. In addition to the ring, a significant portion of the field content also passes through the origin and continues propagating along the axis of symmetry while being highly perturbed.

At the highest velocities, the colliding Q -balls form a clear destructive interference pattern analogous to that seen for the case of small gauge coupling (Fig. 2). However, after the collision, the fields emerge primarily in the form of Q -rings which propagate away from the axis of symmetry. In addition, a scalar radiation pattern can be observed in the vicinity of the origin. This situation is depicted in Fig. 6 for solution LogC at $v = 0.9$, and we have found this phenomenon to be present up to a collision velocity of at least $v = 0.95$. This contrasts what is observed for nongauged Q -balls where high-velocity collisions primarily exhibit

free-passage behavior. Although computational constraints prevent us from exploring boosts much beyond this range (in part due to the extreme field gradients of the boosted Q -balls at these velocities), one can conclude that high-velocity collisions of gauged Q -balls can be considerably less elastic than collisions of their nongauged counterparts.

Another challenge is to determine the ultimate fate of the observed Q -rings. While we have made some effort to track the long-term evolution of these structures, the nature of the collision tends to see these remnants propagating away at large velocities and reaching large coordinate distances. While the change of coordinates (22)–(23) can prevent these components from exiting the domain entirely,

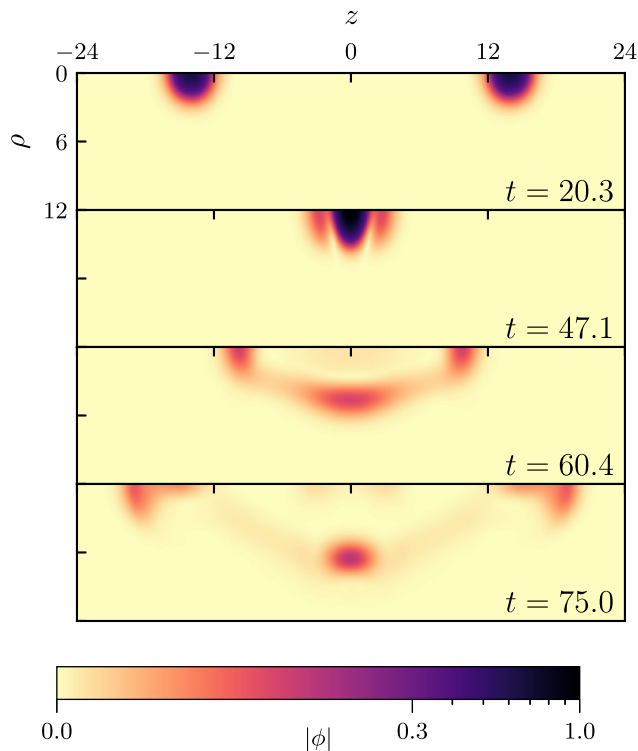


FIG. 5. Evolution of the scalar field modulus $|\phi|$ for a collision of solutions of type LogC with equal charge, velocity $v = 0.55$, and phase difference $\alpha = 0$. The Q -balls collide at $t \approx 45$. After the collision, the field content contains a mixture of on-axis and off-axis components. Note that a hybrid color map is used: field values below $|\phi| = 0.3$ are mapped linearly to zero while values above this threshold are mapped logarithmically to the field maximum.

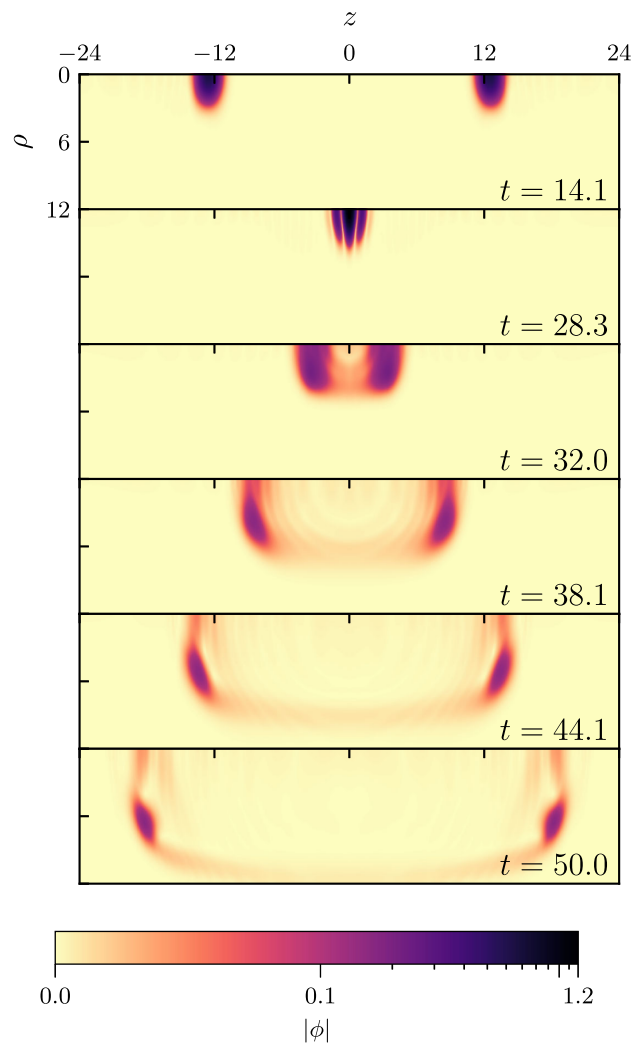


FIG. 6. Evolution of the scalar field modulus $|\phi|$ for a collision of solutions of type LogC with equal charge, velocity $v = 0.9$, and phase difference $\alpha = 0$. The Q -balls collide at $t \approx 27$. After the collision, a scalar radiation pattern appears (fourth panel) and the field content predominantly takes the form of two Q -rings. Note that a hybrid color map is used: field values below $|\phi| = 0.1$ are mapped linearly to zero while values above this threshold are mapped logarithmically to the field maximum.

they become increasingly compactified as the evolution proceeds. When combined with our use of Kreiss-Oliger dissipation for numerical stability, this effectively decreases the numerical resolution of our simulations and increases the global error (as measured, for instance, by an increase in the total constraint violation). As such, it is difficult to conclusively determine the long-term behavior of these structures far from the origin, but we make the general observation that they tend to reach a maximum radius before collapsing back inward toward the axis of symmetry. We therefore conjecture that the gauged Q -rings formed in this way are transient objects (even if the growth of error prevents us from making this statement definitively).

Next, we discuss the effects of phase difference for collisions involving solution LogC. Similar to the case of nongauged Q -balls, the main effect of altering the phase is to induce charge transfer during the collision. However, the large electric charge associated with LogC produces several novel effects. The first is the absence of charge transfer at small collision velocities $v \lesssim 0.3$. Similar to the case when $\alpha = 0$, the Coulomb repulsion prevents the scalar field of each Q -ball from significantly interacting and so the charge transfer process is never observed. At larger velocities, the Q -balls have sufficient kinetic energy to fully interact and the result is a net transfer of charge in a manner similar to the case of small gauge coupling.

One significant difference between charge transfer in the small- and large-coupling case is the final fate of the Q -balls after the collision. In the case of small gauge coupling, the Q -balls typically propagate away after the collision and retain a coherent shape (though occasionally leaving behind a small remnant Q -ball along the axis of symmetry). However, for the case of solution LogC (for example), the most common outcome is that the Q -balls created during the charge transfer process will quickly break apart into smaller components. This phenomenon is depicted in Fig. 7 for a collision involving solution LogC with a phase difference of $\alpha = \pi/4$ and velocity $v = 0.5$. Initially, the Q -balls are Lorentz-boosted toward each other and collide at $t \approx 50$. In this process, approximately 35% of the charge is transferred. As the larger Q -ball is formed, it is also highly perturbed, inducing its decay into smaller Q -balls and Q -rings. Depending on the collision parameters, this instability can manifest in a number of different ways such as by breaking apart into smaller Q -balls, into Q -rings, or into a combination of Q -balls and Q -rings. This phenomenon is presumably due to the reduced parameter space of stable solutions which are allowed when the gauge coupling is large [23].

In general, we find that the charge transfer is maximal at intermediate velocities $0.4 \lesssim v \lesssim 0.6$ for solution LogC. At higher velocities, the effect is still observed but the amount of charge transfer is reduced (for example, the collision of solution LogC at $v = 0.7$, $\alpha = \pi/4$ results in $\sim 10\%$ of the charge transferred while the same collision at

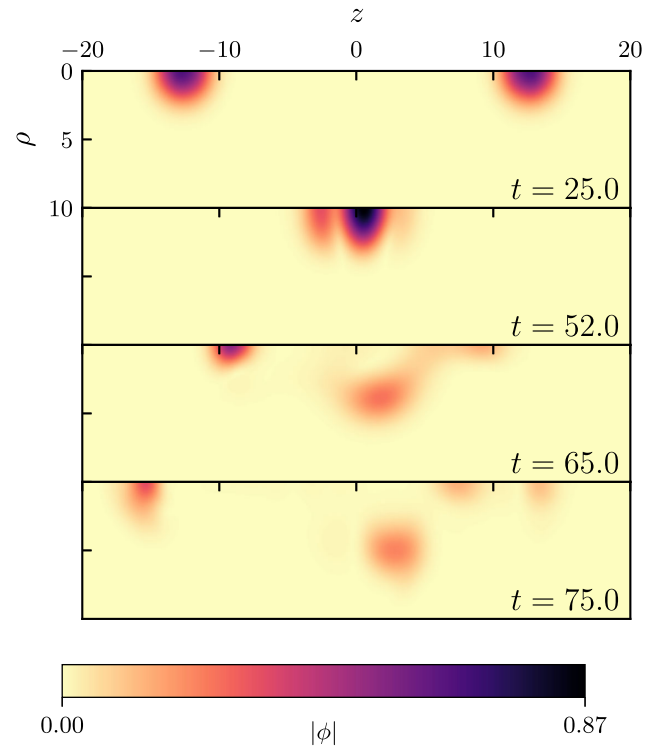


FIG. 7. Evolution of the scalar field modulus $|\phi|$ for a collision of solutions of type LogC with equal charge, velocity $v = 0.5$, and phase difference $\alpha = \pi/4$. The Q -balls collide at $t \approx 50$ and transfer charge (as can be seen in the second panel). After the collision, the larger Q -ball created in this process quickly breaks apart into smaller components which propagate on and away from the axis of symmetry. The smaller Q -ball travels toward $z = -\infty$ while highly perturbed.

$v = 0.9$ results in only $\sim 1\%$ transferred). At these higher velocities, the charge transfer manifests through slight asymmetries in the size and trajectory of the Q -ring pattern. An example of this behavior for solution LogC at $v = 0.7$, $\alpha = \pi/4$ is given in the Appendix (Fig. 14).

We have tested the amount of charge transfer at different phase differences in the range $\alpha \in (0, \pi)$, finding that the transfer is maximal for $\alpha \lesssim \pi/4$. The general phenomena associated with charge transfer is similar for all α tested, though the individual dynamics may differ slightly depending on the collision parameters. However, one exception to the previously described behavior is for the case of $\alpha = \pi$. Similar to what has been observed for small gauge coupling, these out-of-phase Q -balls tend to experience a total repulsion at the moment of impact: the fields are momentarily compressed before the Q -balls “bounce back” and form Q -balls or Q -rings in manner symmetric about $z = 0$ (i.e., there is no charge transfer).

Finally, let us discuss Q -ball/anti- Q -ball interactions at large gauge coupling. As was the case for small gauge coupling, the general outcome of such collisions is the annihilation of charge. However, unlike the case for equal-charge collisions, the oppositely charged Q -balls now

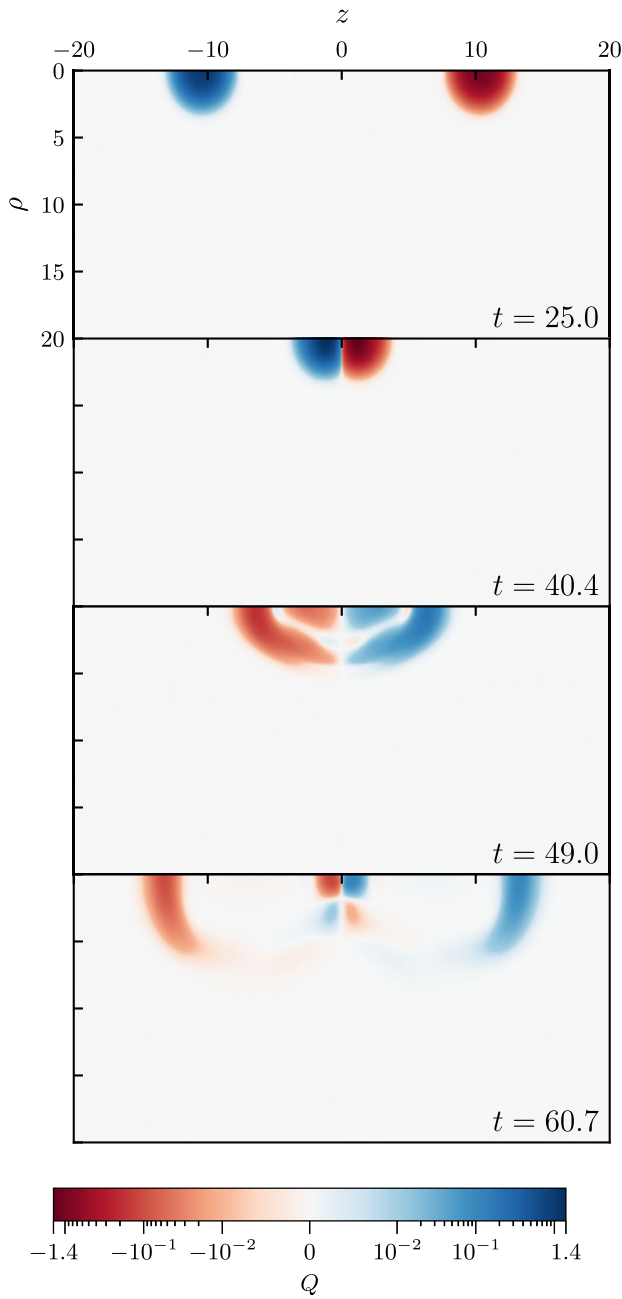


FIG. 8. Evolution of the Noether charge Q for a collision of solutions of type LogC with opposite charge, velocity $v = 0.6$, and phase difference $\alpha = 0$. The Q -balls collide at $t \approx 40$ and partially annihilate charge. After the collision, a significant portion of the charge content continues propagating along the axis of symmetry while a remnant of mixed positive and negative charge is left behind at the origin. Note that a hybrid color map is used: charge values below $|Q| = 10^{-2}$ are mapped linearly to zero while values above this threshold are mapped logarithmically to the charge maximum.

experience an attractive Coulomb force which leads to acceleration prior to the moment of impact; this effect is most noticeable at low velocities. This can lead to an increase in the effective collision velocity as discussed previously.

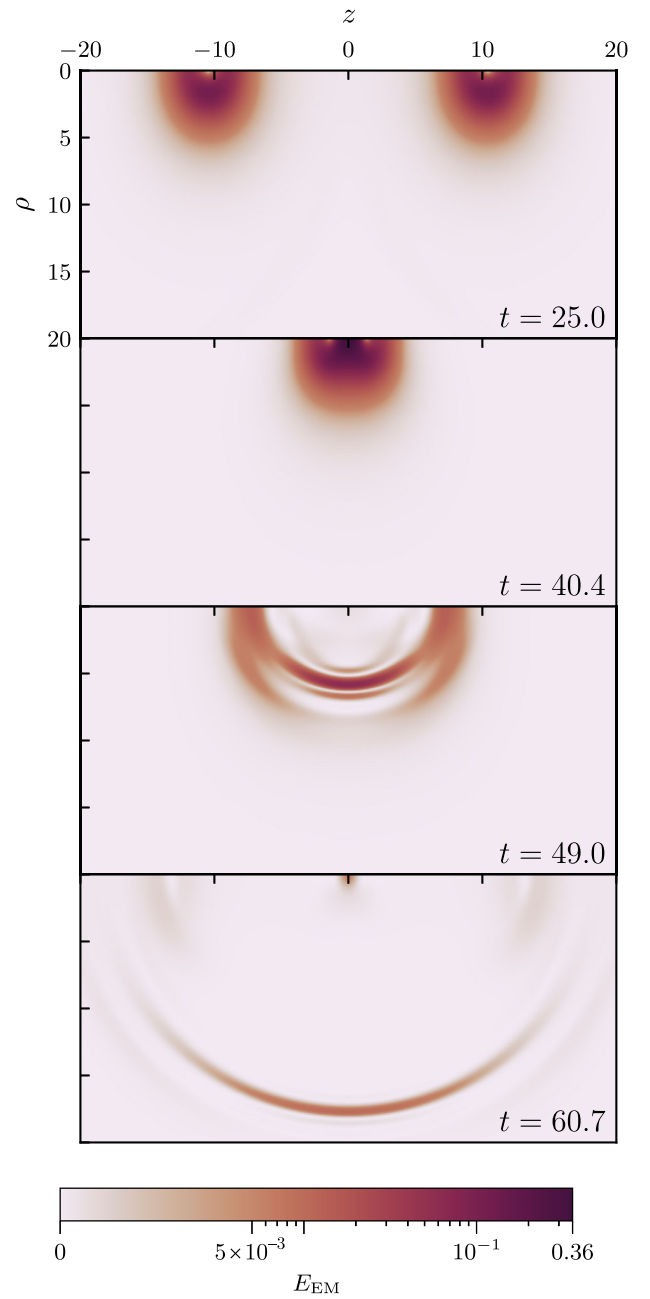


FIG. 9. Evolution of the electromagnetic field energy E_{EM} for a collision of solutions of type LogC with opposite charge, velocity $v = 0.6$, and phase difference $\alpha = 0$. The Q -balls collide at $t \approx 40$ and partially annihilate charge. After the collision, a quasispherical pulse of electromagnetic energy emanates from the origin. Note that a hybrid color map is used: energy values below $E_{EM} = 5 \times 10^{-3}$ are mapped linearly to zero while values above this threshold are mapped logarithmically to the energy maximum.

Plotted in Fig. 8 is the Noether charge Q for a collision involving solution LogC with opposite charge, velocity $v = 0.6$, and phase difference $\alpha = 0$. The Q -balls collide at $t \approx 40$ and partially annihilate. After the collision, a portion of each original Q -ball continues propagating along the axis of symmetry. Additionally, there is a small remnant of

mixed charge left behind at the origin which resembles in some ways a charge-swapping Q -ball [15–17]. In this case, approximately $\sim 53\%$ of the initial charge is annihilated during the collision.

The partial charge annihilation which occurs during a Q -ball/anti- Q -ball collision can also result in the production of electromagnetic radiation. To observe this, we compute from (5) the energy contained in the electromagnetic field, which can be written as

$$E_{\text{EM}} = \frac{1}{2} (|\vec{E}|^2 + |\vec{B}|^2), \quad (24)$$

where \vec{E} and \vec{B} are constructed from the components of the gauge field A_μ . The electromagnetic field energy for a collision involving solution LogC with opposite charge, velocity $v = 0.6$, and phase difference $\alpha = 0$ (i.e., the same collision as is plotted in Fig. 8) is plotted in Fig. 9. Initially, the motion of the charged Q -balls dominates the electromagnetic field energy. At the moment of impact, the Q -balls partially annihilate, converting a fraction of their total energy into a pulse of electromagnetic energy which propagates away from the origin. By comparing Figs. 8 and 9, one can see that the outgoing pulse does not correspond to any significant amount of charge. This fact supports our interpretation of the pulse as representing electromagnetic radiation. We note that we have not made an attempt to precisely quantify the amount of electromagnetic radiation produced in this manner. This is due primarily to the technical challenges associated with integrating the energy over arbitrary subregions of the computational domain during adaptive, highly parallelized simulations. However, we comment that the size of the electromagnetic pulse is generally proportional to the amount of annihilation that occurs. For illustrative purposes, we also plot in the Appendix (Fig. 15) a representation of the electric and magnetic fields for the collision depicted in Figs. 8 and 9.

In the general case, we find that the dynamics of Q -ball/anti- Q -ball interactions depend primarily on the collision velocity. At the lowest velocities, the Q -balls tend to pass through each other after partially annihilating, then continue to travel along the axis of symmetry while oscillating weakly. This process is often accompanied by the partial fragmentation of the Q -balls into a small number of Q -balls or Q -rings. At intermediate velocities (e.g., $0.5 \lesssim v \lesssim 0.7$ for solution LogC), the collision becomes more violent: the resulting Q -balls and Q -rings may be greater in number and more strongly oscillatory after the collision. It is also within this intermediate regime that the charge annihilation is found to be maximal. At the highest velocities (e.g., $v \gtrsim 0.7$ for solution LogC), the outcome of the collision is once again dominated by two main Q -balls which continue propagating along the axis of symmetry. These Q -balls are accompanied by long “tails” of the scalar field which

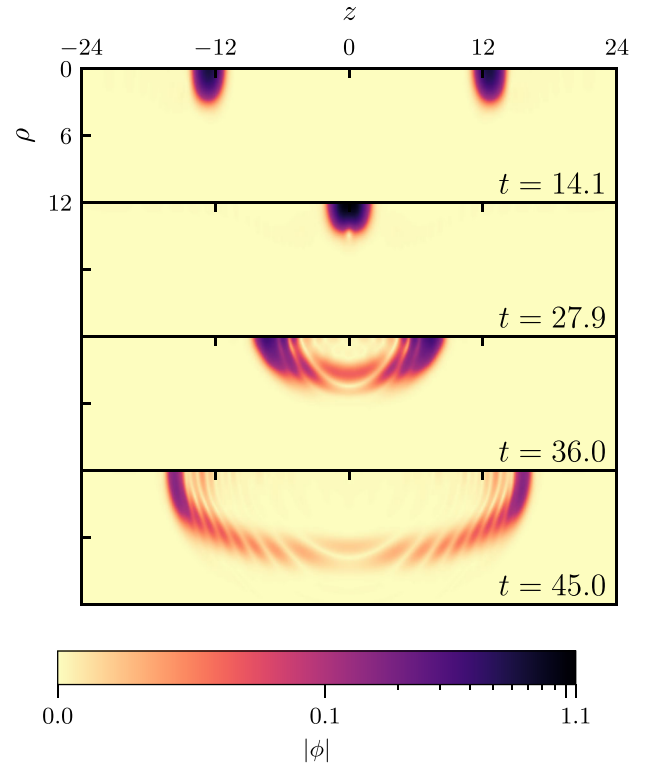


FIG. 10. Evolution of the scalar field modulus $|\phi|$ for a collision of solutions of type LogC with opposite charge, velocity $v = 0.9$, and phase difference $\alpha = 0$. The Q -balls collide at $t \approx 27$ and interfere constructively. After the collision, the Q -balls continue propagating along the axis of symmetry and carry a long “tail” of scalar matter which exhibits an interference fringe pattern. Note that a hybrid color map is used: field values below $|\phi| = 0.1$ are mapped linearly to zero while values above this threshold are mapped logarithmically to the field maximum.

show a clear interference fringe pattern. This behavior is shown in Fig. 10 for solution LogC at $v = 0.9$ with opposite charges and $\alpha = 0$. The amount of charge annihilation is also reduced at high velocities (for example, only $\sim 14\%$ of the charge is annihilated for the collision depicted in Fig. 10).

We have also studied Q -ball/anti- Q -ball collisions of solution LogC at various phase differences up to $\alpha = \pi$. We find that the phase difference has a minimal effect and the phenomena associated with these collisions resembles closely the $\alpha = 0$ case. This suggests that the collision dynamics of gauged Q -balls with gauged anti- Q -balls are determined primarily by the collision velocity, in agreement with the case of small gauge coupling. It is interesting to note that we have not observed any cases of total annihilation where the initial Q -balls are converted completely into radiation. Such a phenomena has been observed in previous studies of nongauged Q -ball collisions for a small range of collision parameters [14]. While total annihilation may still be possible for the gauged case, our analysis suggests that it might likewise occur for only a narrow range of parameters.

We conclude this section by returning to collisions under the polynomial model (20). For this purpose, we focus on solution PolyB in Table I. This solution is notable in that it corresponds to a value of the gauge coupling e which is near the maximum allowed for the polynomial potential, $e_{\max} \approx 0.182$ [32]. Considering first the equal-charge collisions of solution PolyB, we find once again that the Q -balls tend to repel at low velocities. This is in agreement with what has been discussed previously for the logarithmic model. However, for intermediate velocities (e.g., $0.35 \lesssim v \lesssim 0.6$), we observe that the colliding Q -balls can merge into a single Q -ball which remains at the origin. This is accompanied by the emission of charge as the merged Q -ball settles down into a near-stationary configuration. At slightly higher velocities (e.g., $0.65 \lesssim v \lesssim 0.85$), the Q -balls do not form a single stable Q -ball; instead, the fields dissipate shortly after the moment of impact in the form of outgoing waves. This situation is depicted in Fig. 11. For collision velocities $v \gtrsim 0.85$, we find that the majority of the field content emerges along the axis of symmetry after the collision. However, the initial Q -balls are still difficult to distinguish in the aftermath as the field magnitudes are greatly reduced and are also elongated in

the radial direction. This is accompanied by a spherical radiation pattern emanating from the origin. An example of this scenario is depicted in the Appendix (Fig. 16). This lies in contrast to what is observed for the logarithmic model where the dominant field components after the collision take the form of gauged Q -rings (cf. Fig. 6). However, regardless of the final structure, we conclude that the equal-charge collisions of solution PolyB can be considerably inelastic even at collision velocities which are near-luminal.

Turning next to collisions of solution PolyB with a relative phase difference, we find that charge transfer is once again the dominant outcome (as long as the kinetic energy is sufficient to overcome the Coulomb repulsion). Similar to what is observed for solution LogC, the Q -balls created in this manner are often unstable and may quickly fragment after the collision. In some cases, we even find that the instability can manifest via near-complete dispersal of the fields so that the end result of the collision is just one remaining gauged Q -ball. An example of this behavior for solution PolyB is given in the Appendix (Fig. 17). At the highest velocities and for large phase differences, we find that the amount of charge transfer is once again reduced. For collisions of opposite charges, the dynamics are generally independent of the relative phase with the main result being the net annihilation of charge which is maximal at low collision velocities. In contrast to what is observed for solution LogC (cf. Fig. 8), we do not observe the formation of any smaller Q -balls during opposite-charge collisions involving solution PolyB. Instead, the Q -balls tend to continue propagating uniformly along the axis of symmetry, though often being strongly perturbed by the annihilation process.

V. CONCLUSION

In this work, we have performed high-resolution numerical simulations to study head-on collisions of $U(1)$ gauged Q -balls. Focusing on the relativistic regime, we have studied the effects of various parameters (such as collision velocity, relative phase, relative charge, and electromagnetic coupling strength) on the outcome of the collision. Our simulations suggest that the outcome can depend heavily on these parameters, resulting in dynamics which can be quite distinct from those observed during collisions of ordinary (nongauged) Q -balls.

We first examined the dynamics of gauged Q -balls with small gauge coupling. Here it was found that the dynamics for equal-charge collisions can generally be divided into three regimes (the “merger”, “fragmentation,” and “elastic” regimes) depending on the collision velocity. We also studied the effect of phase-difference and opposite-charge collisions, finding evidence for charge transfer and annihilation, respectively. These findings are consistent with what has been previously reported for ordinary (nongauged) Q -balls. Overall, these results suggest that gauged Q -balls with small gauge coupling can behave like nongauged Q -balls during head-on collisions.

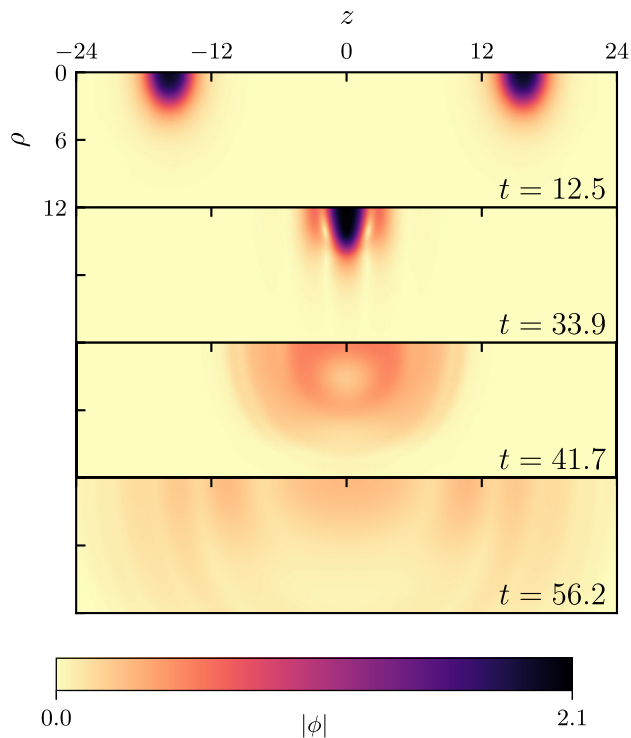


FIG. 11. Evolution of the scalar field modulus $|\phi|$ for a collision of solutions of type PolyB with equal charge, velocity $v = 0.75$, and phase difference $\alpha = 0$. The Q -balls collide at $t \approx 33$ and form a destructive interference pattern. After the collision, it becomes difficult to distinguish any component of the field which clearly resembles a Q -ball. Instead, the field content appears to dissipate in the form of near-spherical waves which emanate from the origin.

Turning to the case of large gauge coupling, we find that collisions of gauged Q -balls can lead to distinct dynamical behavior due to the influence of the electromagnetic field. For equal-charge collisions, the Coulomb force can cause a repulsion which prevents the scalar field of each Q -ball from reaching a state of significant interaction. This occurs at low collision velocities. At higher velocities, we find that collisions are rarely an elastic process; instead, the main outcome is often a fragmentation of the colliding Q -balls into several smaller gauged Q -balls or Q -rings. This effect persists even at collision velocities very close to the speed of light. Studying the effect of phase difference on the collision outcome, we observe evidence for charge transfer. However, the gauged Q -balls created during this process are often unstable and tend to quickly break apart into smaller components. For the case of opposite-charge collisions, we find partial annihilation of the gauged Q -balls to be a generic outcome which can lead to the production of an electromagnetic radiation pulse. Having studied these behaviors using both polynomial and logarithmic scalar field potentials, we find that the collision dynamics can differ slightly depending on the choice of potential. However, we conclude that the main phenomena associated with gauged Q -ball collisions (such as charge transfer, annihilation, and the inelasticity of the collisions) are generally independent of the specifics of the model.

Since the present study has been limited to axisymmetry, it is interesting to ask how the dynamics may change in fully three-dimensional simulations. This question will be addressed in a future publication. It would also be interesting to consider how quantum effects may influence the dynamics of gauged Q -balls similar to what has recently been done for nongauged Q -balls [33]. Finally, we comment that the results of this work could be extended by considering more general scenarios in axisymmetry (such as collisions between gauged Q -balls with unequal $|Q|$) or by studying in further detail the electromagnetic signal created during the collisions. These scenarios may be relevant for cosmological applications of gauged Q -balls [34–37].

ACKNOWLEDGMENTS

We thank G. Reid for providing valuable advice and feedback. This work was supported by the Natural Sciences and Engineering Research Council of Canada (M. W. C., M. P. K.), the Walter C. Sumner Foundation (M. P. K.), and the Province of British Columbia (M. P. K.). Computing resources were provided by the Digital Research Alliance of Canada and the University of British Columbia.

APPENDIX: SUPPLEMENTAL FIGURES

To supplement the figures presented in the main text, here we provide additional plots which illustrate several interesting cases of gauged Q -ball dynamics.

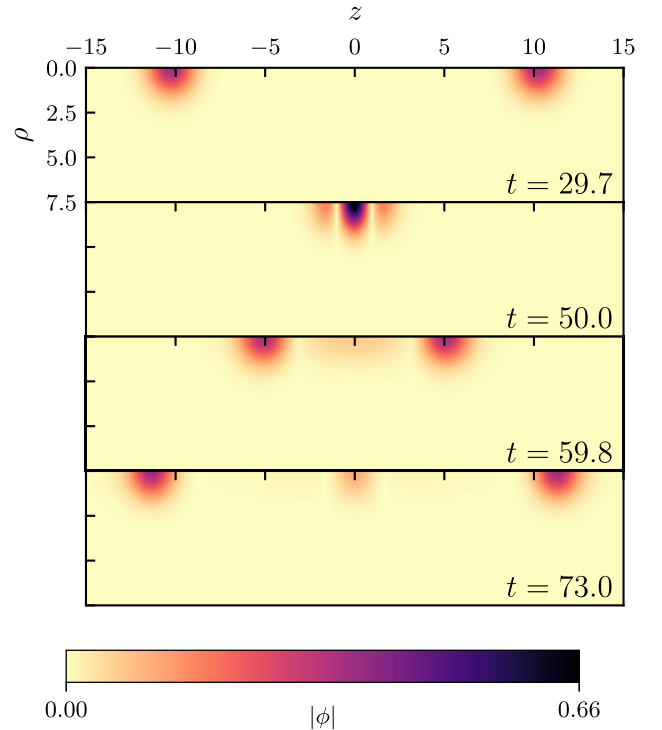


FIG. 12. Evolution of the scalar field modulus $|\phi|$ for a collision of solutions of type LogA with equal charge, velocity $v = 0.5$, and phase difference $\alpha = 0$. The Q -balls collide at $t \approx 50$ and pass through each other, leaving behind a smaller Q -ball remnant which remains perturbed at the origin.

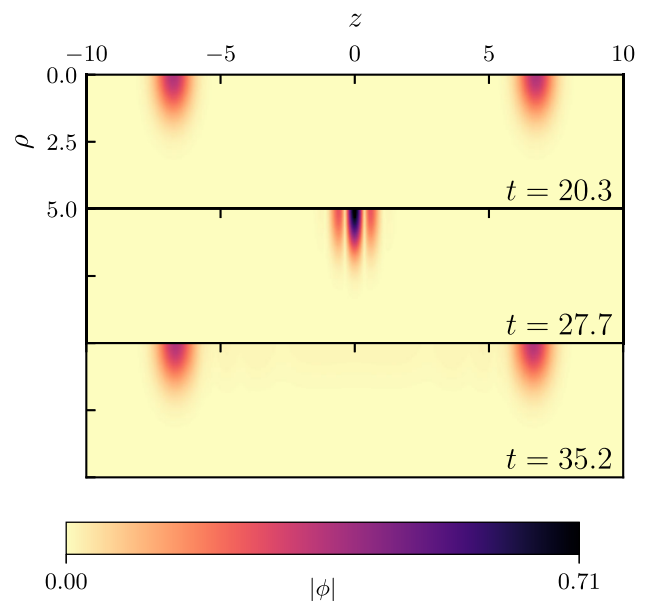


FIG. 13. Evolution of the scalar field modulus $|\phi|$ for a collision of solutions of type LogA with equal charge, velocity $v = 0.9$, and phase difference $\alpha = 0$. The Q -balls collide at $t \approx 27$ and exhibit a destructive interference pattern. After the collision, the Q -balls emerge with profiles nearly identical to their initial state.

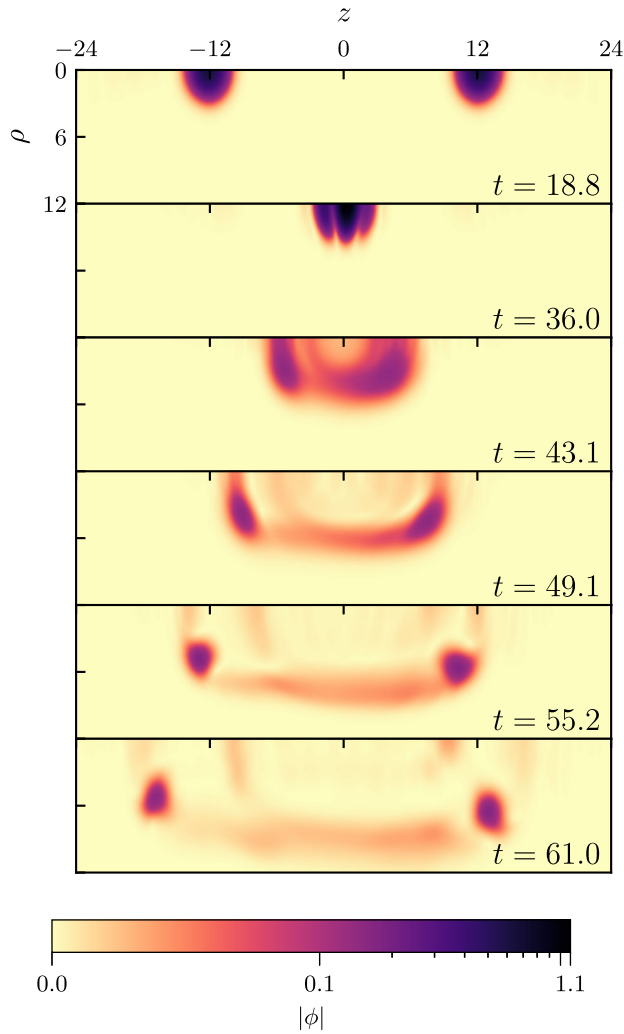


FIG. 14. Evolution of the scalar field modulus $|\phi|$ for a collision of solutions of type LogC with equal charge, velocity $v = 0.7$, and phase difference $\alpha = \pi/4$. The Q -balls collide at $t \approx 36$. After the collision, the field content predominantly takes the form of two Q -rings. In this case, the phase difference manifests as an asymmetry in the dynamics about the plane $z = 0$. Note that a hybrid color map is used: field values below $|\phi| = 0.1$ are mapped linearly to zero while values above this threshold are mapped logarithmically to the field maximum.

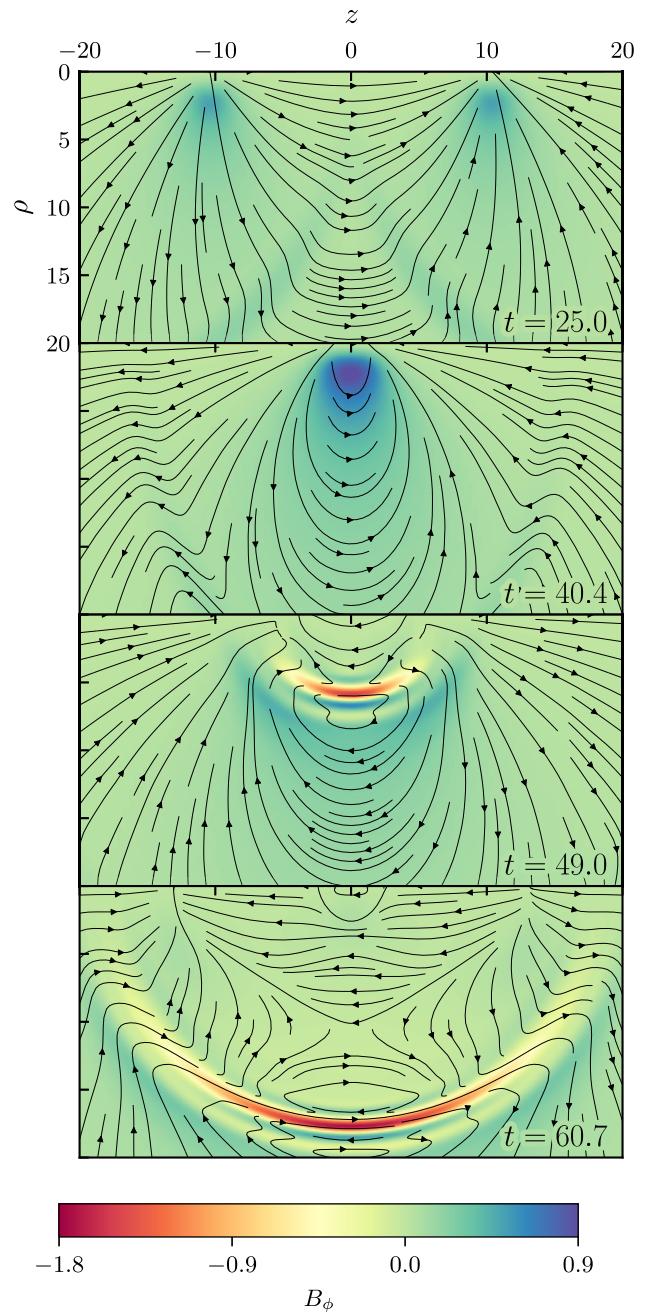


FIG. 15. Evolution of the electric field \vec{E} and the magnetic field \vec{B} for a collision of solutions of type LogC with opposite charge, velocity $v = 0.6$, and phase difference $\alpha = 0$. The magnitude of the only nonzero component of the magnetic field, B_ϕ , is represented using the color map. The orientation of the electric field is represented using streamlines; the corresponding field magnitude is not reflected in the figure. The Q -balls collide at $t \approx 40$ and partially annihilate charge. After the collision, the fields resemble an outgoing wavefront. We note that the small-scale “pulse” which is visible for $\rho \gtrsim 10$ in the first and second panel exists as a technical artefact of the gauged Q -ball initialization procedure at $z = \pm 25$.

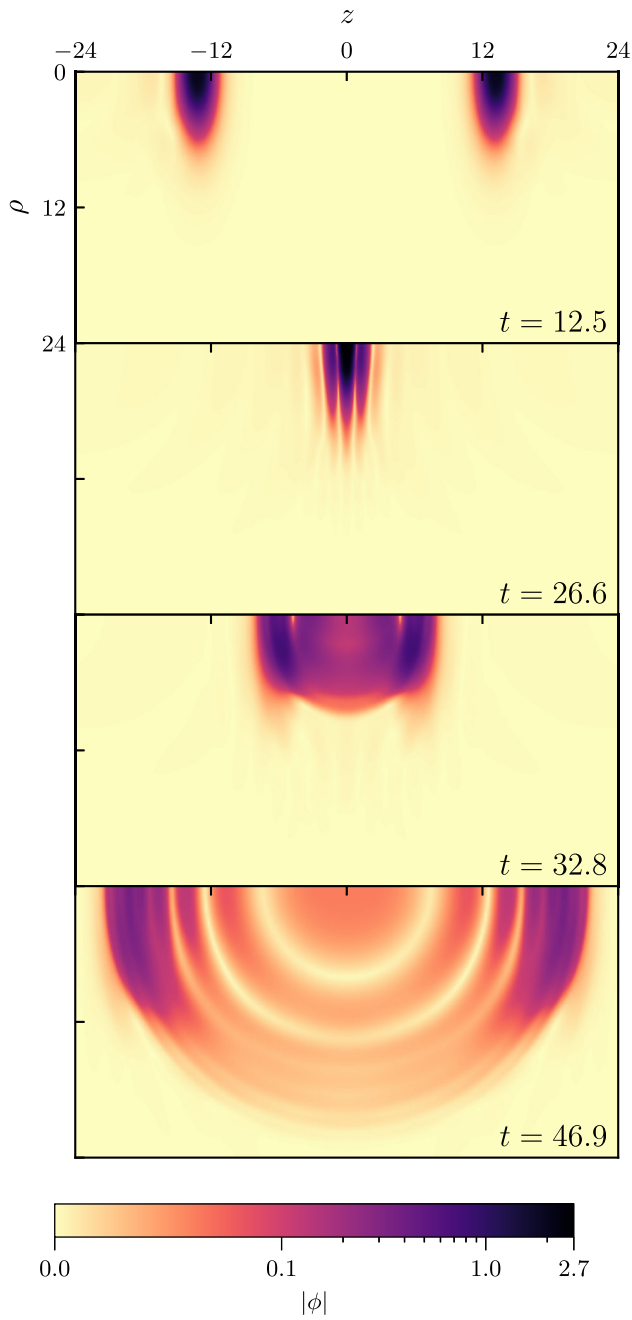


FIG. 16. Evolution of the scalar field modulus $|\phi|$ for a collision of solutions of type PolyB with equal charge, velocity $v = 0.95$, and phase difference $\alpha = 0$. The Q -balls collide at $t \approx 26$ and form a destructive interference pattern. After the collision, the majority of the field content continues traveling along the axis of symmetry and becomes elongated in the radial direction. Note that a hybrid color map is used: field values below $|\phi| = 0.1$ are mapped linearly to zero while values above this threshold are mapped logarithmically to the field maximum.

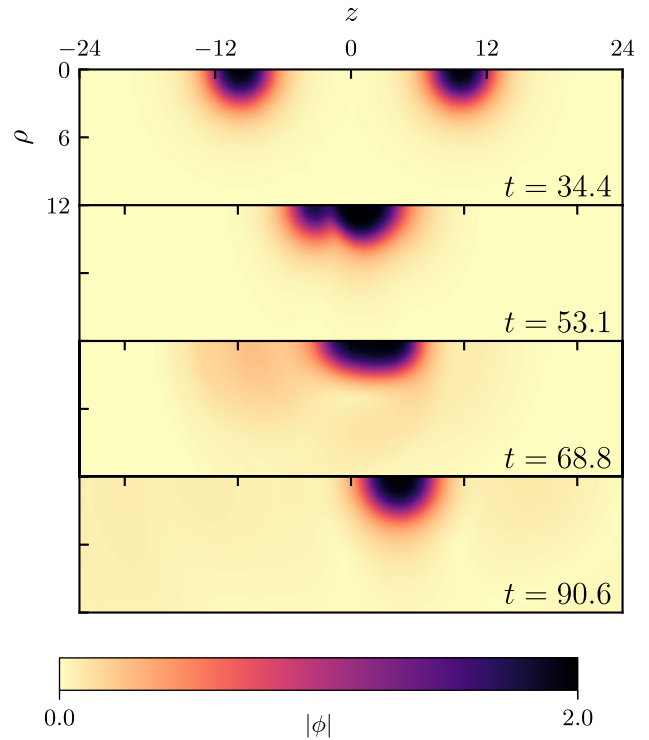


FIG. 17. Evolution of the scalar field modulus $|\phi|$ for a collision of solutions of type PolyB with equal charge, velocity $v = 0.45$, and phase difference $\alpha = \pi/4$. The Q -balls collide at $t \approx 53$ and transfer charge (as can be seen in the second panel). After the collision, the smaller Q -ball created in this process quickly dissipates while the larger Q -ball travels slowly along the axis of symmetry.

- [1] N. Manton and P. Sutcliffe, *Topological Solitons*, 1st ed., Cambridge Monographs on Mathematical Physics (Cambridge University Press, Cambridge, England, 2004).
- [2] Y. M. Shnir, *Topological and Non-Topological Solitons in Scalar Field Theories*, 1st ed., Cambridge Monographs on Mathematical Physics (Cambridge University Press, Cambridge, England, 2018).
- [3] S. Coleman, *Nucl. Phys.* **B262**, 263 (1985); **B269**, 744 (1986).
- [4] E. Y. Nugaev and A. V. Shkerin, *J. Exp. Theor. Phys.* **130**, 301 (2020).
- [5] S. Kasuya and M. Kawasaki, *Phys. Rev. D* **61**, 041301(R) (2000).
- [6] M. Dine and A. Kusenko, *Rev. Mod. Phys.* **76**, 1 (2004).
- [7] A. Kusenko and M. Shaposhnikov, *Phys. Lett. B* **418**, 46 (1998).
- [8] A. Kusenko and P. J. Steinhardt, *Phys. Rev. Lett.* **87**, 141301 (2001).
- [9] E. Radu and M. S. Volkov, *Phys. Rep.* **468**, 101 (2008).
- [10] K. Enqvist and M. Laine, *J. Cosmol. Astropart. Phys.* **08** (2003) 003.
- [11] Y. M. Bunkov and G. E. Volovik, *Phys. Rev. Lett.* **98**, 265302 (2007).
- [12] K. Lee, J. A. Stein-Schabes, R. Watkins, and L. M. Widrow, *Phys. Rev. D* **39**, 1665 (1989).
- [13] M. Axenides, S. Komineas, L. Perivolaropoulos, and M. Floratos, *Phys. Rev. D* **61**, 085006 (2000).
- [14] R. A. Battye and P. M. Sutcliffe, *Nucl. Phys.* **B590**, 329 (2000).
- [15] E. J. Copeland, P. M. Saffin, and S.-Y. Zhou, *Phys. Rev. Lett.* **113**, 231603 (2014).
- [16] Q.-X. Xie, P. M. Saffin, and S.-Y. Zhou, *J. High Energy Phys.* **07** (2021) 062.
- [17] S.-Y. Hou, P. M. Saffin, Q.-X. Xie, and S.-Y. Zhou, *J. High Energy Phys.* **07** (2022) 060.
- [18] T. Multamäki and I. Vilja, *Phys. Lett. B* **482**, 161 (2000).
- [19] T. Multamäki and I. Vilja, *Phys. Lett. B* **484**, 283 (2000).
- [20] J. H. Al-Alawi and W. J. Zakrzewski, *J. Phys. A* **42**, 245201 (2009).
- [21] B. Gutierrez, Relativistic scattering of solitons in nonlinear field theory, Ph.D. thesis, University of British Columbia, 2013.
- [22] G. Dvali, O. Kaikov, F. Kühnel, J. S. Valbuena-Bermúdez, and M. Zantedeschi, *Phys. Rev. Lett.* **132**, 151402 (2024).
- [23] M. P. Kinach and M. W. Choptuik, *Phys. Rev. D* **107**, 035022 (2023).
- [24] I. E. Gulamov, E. Y. Nugaev, A. G. Panin, and M. N. Smolyakov, *Phys. Rev. D* **92**, 045011 (2015).
- [25] J. Heeck, A. Rajaraman, R. Riley, and C. B. Verhaaren, *Phys. Rev. D* **103**, 116004 (2021).
- [26] W. H. Press, S. A. Teukolsky, W. T. Vetterling, and B. P. Flannery, *Numerical Recipes: The Art of Scientific Computing*, 3rd ed. (Cambridge University Press, Cambridge, England, 2007).
- [27] F. Pretorius and M. W. Choptuik, *J. Comput. Phys.* **218**, 246 (2006).
- [28] I. E. Gulamov, E. Y. Nugaev, and M. N. Smolyakov, *Phys. Rev. D* **89**, 085006 (2014).
- [29] P. Bowcock, D. Foster, and P. Sutcliffe, *J. Phys. A* **42**, 085403 (2009).
- [30] B. Schwabe, J. C. Niemeyer, and J. F. Engels, *Phys. Rev. D* **94**, 043513 (2016).
- [31] V. Cardoso, S. Hopper, C. F. B. Macedo, C. Palenzuela, and P. Pani, *Phys. Rev. D* **94**, 084031 (2016).
- [32] A. Y. Loginov and V. V. Gauszhtein, *Phys. Rev. D* **102**, 025010 (2020).
- [33] Q.-X. Xie, P. M. Saffin, A. Tranberg, and S.-Y. Zhou, *J. High Energy Phys.* **01** (2024) 165.
- [34] J.-P. Hong, M. Kawasaki, and M. Yamada, *Phys. Rev. D* **92**, 063521 (2015).
- [35] J.-P. Hong, M. Kawasaki, and M. Yamada, *J. Cosmol. Astropart. Phys.* **08** (2016) 053.
- [36] J.-P. Hong and M. Kawasaki, *Phys. Rev. D* **95**, 123532 (2017).
- [37] S. Jiang, F. P. Huang, and P. Ko, [arXiv:2404.16509](https://arxiv.org/abs/2404.16509).